Strathprints Institutional Repository

Collision Strengths for Nebular [O III] Optical and Infrared Lines

P.J. Storey[1], Taha Sochi[1]⋆ and N.R. Badnell[2]

[1] *University College London, Department of Physics and Astronomy, Gower Street, London, WC1E 6BT*

[2] *Department of Physics, University of Strathclyde, Glasgow, G4 0NG, UK*

ABSTRACT

We present electron collision strengths and their thermally averaged values for the nebular forbidden lines of the astronomically abundant doubly-ionized oxygen ion, O^{2+}, in an intermediate coupling scheme using the Breit-Pauli relativistic terms as implemented in an R-matrix atomic scattering code. We use several atomic targets for the R-matrix scattering calculations including one with 72 atomic terms. We also compare with new results obtained using the intermediate coupling frame transformation method. We find spectroscopically significant differences against a recent Breit-Pauli calculation for the excitation of the [O III] $\lambda 4363$ transition but confirm the results of earlier calculations.

Key words: atomic data – atomic processes – radiation mechanisms: non-thermal – infrared: general – planetary nebulae: general.

1 INTRODUCTION

The forbidden lines of O^{2+} are among the most important features in the spectra of photoionized plasmas which include, *inter alia*, H II regions and planetary nebulae. The exceptional brightness of the strongest [O III] lines means that they can be used to determine the oxygen abundances and physical conditions in the Milky Way and other galaxies out to cosmological distances that reach redshifts of more than $z = 3$ (Maiolino *et al* 2008).

It has been recently suggested (Nicholls *et al* 2012) that the elemental abundance and electron temperature anomalies seen in the analysis of the planetary nebula spectra, where considerable differences have been observed between the results obtained from the collisionally-excited lines (CEL) and those obtained from the optical recombination lines (ORL), might be resolved by using non Maxwell-Boltzmann (MB) distributions for the energies of the free electrons. The κ distribution, which is widely used in the analysis of solar data, was proposed as a replacement for the MB distribution to resolve this issue. If the electron distributions are generally non-Maxwellian in nebulae it would affect the analysis of [O III] lines significantly and reliable collision strength data are needed to compute the effective collision strengths for collisional excitation and de-excitation.

The proposal that the electron energy distribution in planetary nebulae is not Maxwellian dates back to the 1940s at least where Hagihara (1944) proposed that the velocity

distribution of free electrons in gaseous assemblies, such as those found in planetary nebulae, deviates significantly from the Maxwellian. Bohm & Aller (1947) argued against Hagihara and concluded that any deviation from the Maxwellian equilibrium distribution is very small. The essence of Bohm and Aller's argument is that for typical planetary nebulae conditions of electron temperature of about 10000 K and electron number density of about 10^4 cm^{-3}, the thermalization process of elastic collisions between an electron and other electrons and ions is by far the most frequent event and typically occurs once every second, while other processes that shift the system from its thermodynamic equilibrium, like inelastic scattering with other ions that leads to metastable excitation or recapture, occur at much larger time scales estimated to be months or even years. Bohm and Aller also indicated the significance of any possible deviation from a Maxwellian distribution on derived elemental abundances.

Although there have been many studies related to collision strengths of O^{2+}, as we will discuss in the coming paragraphs, some of the previous data have limitations. For example, some of these data are produced in an *LS*-coupling scheme while others are based on approaches that do not adequately treat resonance phenomena.

Before the advent of close-coupling codes there were several calculations of collision strengths for excitation of the O III forbidden lines that did not incorporate resonance effects (Czyzak *et al* 1968; Seaton 1975; Bhatia *et al* 1979).

The first close-coupled collision strengths were obtained by Baluja *et al* (1980) for some of the semi-forbidden inter-

---

⋆ E-mail: t.sochi@ucl.ac.uk.

combination transitions of O III using the R-matrix method (Berrington *et al* 1974, 1987; Hummer *et al* 1993; Berrington *et al* 1995). They included all channels with configurations $1s^2\,2s^2\,2p^2$, $1s^2\,2s\,2p^3$ and $1s^2\,2p^4$ in the expansion of the wavefunction. They also used three pseudo-orbitals ($\overline{3}$s, $\overline{3}$p and $\overline{3}$d) and allowed for configuration interaction in the included states with the addition of correlation terms in the total wavefunction.

Ho & Henry (1983) also used the close coupling approximation with configuration interaction in the target wavefunction to compute the collision strengths of some of O III transitions in LS-coupling. They employed a mix of spectroscopic and correlation Hartree-Fock orbitals to describe their target.

Relatively extensive work was done by Aggarwal (1983, 1985) who computed collision strengths of O III transitions between the fine structure levels using configuration interaction target wavefunctions. He transformed LS-coupling reactance matrices obtained from R-matrix calculations to pair coupling with the program JAJOM (Saraph 1978). The results were obtained with a fine energy mesh up to 5.16 Rydberg where a complex resonance structure was observed on the entire mesh.

Aggarwal (1993) used an elaborate configuration interaction target described by Aggarwal & Hibbert (1991) and the R-matrix method in LS-coupling to compute effective collision strengths for some inelastic transitions of O III between 26 LS-coupled states of six configurations over a wide range of electron temperature (2500-200000 K). They employed the standard and no-exchange R-matrix codes on a fine energy mesh that reveals the resonance structure. This work was extended by Aggarwal & Keenan (1999), who computed the collision strengths for the transitions between the fine structure levels using the R-matrix method including all partial waves with $L \leqslant 40$ to ensure convergence. Aggarwal & Keenan (1999) transformed the LS reactance matrices obtained by Aggarwal (1993) into pair coupling using JAJOM (Saraph 1978) where necessary. They only tabulated fine-structure collision strengths for some transitions, pointing out that in pair coupling, if one of the terms in a transition has spin zero and hence $J = L$, e.g. ^{3}P – ^{1}D, the fine-structure collision strengths are proportional to the statistical weight of the non-zero spin states, in this example the ^{3}P$_J$ levels.

Lennon & Burke (1994) did extensive work on O^{2+} collision strengths for the transitions between the fine structure levels, as part of a wider investigation on the carbon isoelectronic ions, using the R-matrix method, where the CIV3 configuration interaction code (Hibbert 1975) was used to generate the target wavefunctions. The target included 12 states belonging to 3 configurations ($1s^2\,2s^2\,2p^2$, $1s^2\,2s\,2p^3$ and $1s^2\,2p^4$). They also transformed to pair coupling in the same way as Aggarwal & Keenan (1999) described above. They presented a sample of Maxwellian based effective collision strengths in the temperature range $10^3 - 10^5$ K.

Recently, Palay *et al* (2012) made the first calculation of collision strengths for the O III forbidden transitions using a relativistic Breit-Pauli (BP) R-matrix method with resolved resonance structures. They used 22 configurations (3 spectroscopic and 19 correlation) to describe the target. Like most of the previous studies, they have also presented sam-

ples of the Maxwellian averaged effective collision strengths which were also computed at temperatures down to 100 K.

The most recent R-matrix calculations (Lennon & Burke 1994; Aggarwal & Keenan 1999; Palay *et al* 2012) generally agree to within 10% for the thermally averaged collision strengths for the forbidden transitions among the five lowest levels. An exception to this generally close agreement is for the transitions from the lowest three ^{3}P$_J$ levels to the ^{1}S$_0$ state. The recent results of Palay *et al* (2012) differ significantly from those of earlier workers. The excitation mechanism of the ^{1}S$_0$ level is important because the ^{1}S$_0 \rightarrow\,^1$D$_2$ $\lambda4363$ line is widely used to infer the electron temperature in H II regions and planetary nebulae. If a κ distribution of electron energies is assumed, the number of free electrons capable of exciting the ^{1}S$_0$ state would be increased relative to a MB distribution which would affect the derived O^{2+} abundance.

The aim of the present paper is twofold. Firstly we make a Breit-Pauli R-matrix calculation of the O^{2+} collision strengths with an independently derived target configuration basis to compare with previous work, especially the only other Breit-Pauli results from Palay *et al* (2012). Secondly we attempt to place realistic error estimates on our results by examining the effect of several factors on our results. We discuss the convergence of our calculation as the number of target states is increased. Our largest target includes significant contributions to the dipole polarizability of the three energetically lowest terms. We also consider the effect of Gailitis averaging of the collision strengths close to the excitation thresholds, especially for excitation of the ^{3}P$_1$ level between the ^{3}P$_1$ and ^{3}P$_2$ thresholds. We additionally compare the results of the Breit-Pauli calculation with those obtained using the Intermediate Coupling Frame Transformation (ICFT) R-matrix method (Griffin, Badnell & Pindzola 1998). This method is based on transforming the non-physical LS-coupled reactance matrices, to compute collision strengths in intermediate coupling.

The calculation described in the following sections is constructed to provide accurate results for the excitation of the optical and infrared forbidden transitions among the five lowest levels of O^{2+} at temperatures typical of the photoionized plasmas in nebulae. We compute collision strengths up to ≈ 1.3 Rydberg free electron energy relative to the ground level and Maxwell-Boltzmann averaged collision strengths from 100 K to 25000 K. We set the lower limit of temperature at 100 K to reflect the suggestion that planetary nebulae may contain material of very low temperature, in the form of knots or clumps, within the main nebular body which is at a much higher temperature (Liu *et al* 2000; Zhang *et al* 2004; Liu *et al* 2006). These multi-component nebular models have gathered momentum recently as they seem to offer the most satisfactory explanation to the long-standing problem of ORL-CEL abundance and temperature inconsistency (Storey & Sochi 2014). As for the upper limit, it is justified by the fact that the estimation of the maximum temperature for photoionized nebulae is around 20000-25000 K.

The main tools used in this investigation are the Autostructure code[1] (Eissner *et al* 1974; Nussbaumer & Storey

---

[1] See Badnell: Autostructure write-up on WWW. URL: amdpp.phys.strath.ac.uk/autos/ver/WRITEUP.

Table 1. The configuration basis used to define the scattering target. The $1s^2$ core is to be understood in all configurations. The bar signifies a correlation orbital.

$2s^2\ 2p^2,\ 2s\ 2p^3,\ 2p^4$
$2s^2\ 2p\ \overline{3l};\ l = 0, 1, 2$
$2s\ 2p^2\ \overline{3l};\ l = 0, 1, 2$
$2p^3\ \overline{3l};\ l = 0, 1, 2$
$2s^2\ \overline{3l}\ \overline{3l}',\ l, l' = 0,1,2$
$2s\ 2p\ \overline{3l}\ \overline{3l}',\ l, l' = 0,1,2$
$2p^2\ \overline{3l}\ \overline{3l}',\ l, l' = 0,1,2$
$2s^2\ 2p\ \overline{4f},\ 2s\ 2p^2\ \overline{4f},\ 2p^3\ \overline{4f}$
$2s^2\ \overline{3d}\ \overline{4f},\ 2s\ 2p\ \overline{3d}\ \overline{4f},\ 2p^2\ \overline{3d}\ \overline{4f}$
$2s^2\ \overline{4f}^2,\ 2s\ 2p\ \overline{4f}^2,\ 2p^2\ \overline{4f}^2$

Table 2. Orbital scaling parameters, λ_{nl}, for Autostructure input. The rows stand for the principal quantum number n, while the columns stand for the orbital angular momentum quantum number l.

	s	**p**	**d**	**f**
1	1.44889			
2	1.22418	1.18282		
$\overline{3}$	-0.80508	-0.61905	-1.04731	
$\overline{4}$				-1.87410

1978; Badnell 2011) to define and elaborate the atomic target and the UCL-Belfast-Strathclyde R-matrix code[2] (Berrington *et al* 1995) to do the actual scattering calculations. We compare our results with earlier calculations and also assess the reliability of our results.

2 COMPUTATION

In the following we outline the computational methods used in this work.

2.1 The O^{2+} target

We used the Autostructure code (Badnell 2011) to generate the target radial functions required as an input to the first stage of the R-matrix code. The radial data were generated using thirty-nine configurations containing seven orbitals; three physical (1s, 2s and 2p) and four correlation orbitals ($\overline{3s}$, $\overline{3p}$, $\overline{3d}$, $\overline{4f}$). These configurations are given in Table 1. An iterative optimization variational protocol was used to obtain the orbital scaling parameters, λ_{nl}, which are given in Table 2. The correlation orbitals are calculated in a Coulomb potential with central charge $8|\lambda_{nl}|$.

In the scattering calculations, targets with differing numbers of target states were used, with the largest having 72 terms which are listed in Table 3. Calculations were also made with the first 10 and 20 terms from this list as discussed in more detail below. Comparing the statistically

weighted oscillator strengths, gf, in the length and velocity formulations for all the strong allowed transitions between the $2s^2\ 2p^2$ and $2s\ 2p^3$ configurations, we find excellent agreement with an average difference of 2.6%. Good agreement between the length and velocity results is a necessary but not sufficient condition for ensuring the quality of the target wave functions. These transitions also make the largest contributions to the dipole polarizabilities of the three lowest terms.

The 72 terms listed in Table 3 were chosen to include all those correlation configurations that contribute significantly to the dipole polarizability of the three lowest terms. The main contributions come from $2s^2\ 2p\ \overline{3d}$ configuration. The contribution of states outside the $n = 2$ complex to the dipole polarizabilities of the ^3P, ^1D and ^1S terms is 37%, 37% and 60% respectively. In Table 4 we list the energies of the 18 levels of the $n = 2$ complex configurations. We show theoretical energies which include one- and two-body fine-structure interactions (E_{th2}) and those which only include the spin-orbit interaction (E_{th1}), the latter being the only fine-structure interactions included in the version of the R-matrix code that we use (see footnote 2). We return to the effect of omitting two-body fine structure interactions in section 3.

2.2 The Scattering Calculations

We made several calculations with increasing numbers of target states, both with Breit-Pauli and the Intermediate Coupling Frame Transformation R-matrix methods. The target radial functions were supplied as a radial grid format rather than Slater type orbital format where the radial file was generated by Autostructure. The inner region radius (RA) in the R-matrix formulation was 9.315 au. Twelve continuum basis functions were used to represent the wavefunctions in the inner region. This choice was based on convergence tests and with experience from previous work on the $C^+ + e^-$ system (Sochi 2012; Sochi & Storey 2013). The maximum value of $2J$ for the $(N + 1)$-electron problem was chosen to be 19 although 15 was found to be sufficient for convergence of the collision strengths for the forbidden transitions of interest here.

As indicated previously, we made three sets of calculations using the configuration basis described in section 2.1 with 10-, 20- and 72-terms using both the BP and ICFT approaches. These three targets comprise 18, 34 and 146 fine-structure levels respectively. The main purpose of using several targets is to have an estimate of the error in the final results from observing the convergence of the results with different numbers of target terms. For all three targets, the $(N + 1)$-electron wavefunction contains all possible configurations formed from the 39 configurations of the N-electron target combined with any of the orbitals, spectroscopic and correlation. There are 102 such $(N + 1)$-electron configurations.

Experimental energies obtained from the National Institute of Standards and Technology (NIST)[3] were used in place of theoretical ones to ensure correct positioning of

---

[2] See Badnell: R-matrix write-up on WWW. URL: amdpp.phys.strath.ac.uk/UK_RmaX/codes/serial/WRITEUP.

[3] See NIST website: www.nist.gov.

Table 3. Target terms and energies, E, calculated by Autostructure using the configuration basis listed in Table 1. The $1s^2$ core is suppressed from all configurations. All these terms are included in the 72-term target, while for the smaller targets (10- and 20-term) only the first 10 and 20 terms respectively are included.

Index	Configuration	Term	E (cm^{-1})	Index	Configuration	Term	E (cm^{-1})
1	$2s^2\ 2p^2$	^3P	0.0	37	$2s\ 2p^2\ \overline{3}p$	$^1S^o$	483995
2	$2s^2\ 2p^2$	^1D	21257	38	$2s\ 2p^2\ \overline{3}p$	$^3P^o$	485363
3	$2s^2\ 2p^2$	^1S	45630	39	$2s\ 2p^2\ \overline{3}s$	^3S	486363
4	$2s\ 2p^3$	$^5S^o$	58948	40	$2s\ 2p^2\ \overline{3}p$	$^1P^o$	486594
5	$2s\ 2p^3$	$^3D^o$	121133	41	$2s\ 2p^2\ \overline{3}p$	$^3D^o$	491627
6	$2s\ 2p^3$	$^3P^o$	144640	42	$2s\ 2p^2\ \overline{3}s$	^3P	496357
7	$2s\ 2p^3$	$^1D^o$	190314	43	$2s\ 2p^2\ \overline{3}p$	$^3P^o$	498566
8	$2s\ 2p^3$	$^3S^o$	199693	44	$2s\ 2p^2\ \overline{3}p$	$^3S^o$	503468
9	$2s\ 2p^3$	$^1P^o$	214885	45	$2s\ 2p^2\ \overline{3}s$	^1P	506149
10	$2p^4$	^3P	287613	46	$2s\ 2p^2\ \overline{3}s$	^1S	508564
11	$2s^2\ 2p\ \overline{3}p$	^1P	301182	47	$2s\ 2p^2\ \overline{3}p$	$^1D^o$	509665
12	$2p^4$	^1D	302782	48	$2s\ 2p^2\ \overline{3}p$	$^1P^o$	526999
13	$2s^2\ 2p\ \overline{3}p$	^3D	306265	49	$2s^2\ 2p\ \overline{3}d$	$^3F^o$	539361
14	$2s^2\ 2p\ \overline{3}s$	$^3P^o$	309248	50	$2p^3\ \overline{3}p$	^5P	542552
15	$2s^2\ 2p\ \overline{3}p$	^3S	310788	51	$2s^2\ 2p\ \overline{3}d$	$^1D^o$	550865
16	$2s^2\ 2p\ \overline{3}p$	^3P	315730	52	$2p^3\ \overline{3}s$	$^5S^o$	551832
17	$2s^2\ 2p\ \overline{3}s$	$^1P^o$	323156	53	$2p^3\ \overline{3}p$	^3P	553504
18	$2s^2\ 2p\ \overline{3}p$	^1D	328464	54	$2p^3\ \overline{3}p$	^3D	567272
19	$2s^2\ 2p\ \overline{3}p$	^1S	345567	55	$2p^3\ \overline{3}p$	^1P	567946
20	$2p^4$	^1S	351203	56	$2p^3\ \overline{3}p$	^3F	568179
21	$2s\ 2p^2\ \overline{3}p$	$^3S^o$	372370	57	$2p^3\ \overline{3}p$	^1F	570684
22	$2s\ 2p^2\ \overline{3}p$	$^5D^o$	376169	58	$2s^2\ 2p\ \overline{3}d$	$^3P^o$	572129
23	$2s\ 2p^2\ \overline{3}s$	^5P	379161	59	$2s^2\ 2p\ \overline{3}d$	$^3D^o$	578854
24	$2s\ 2p^2\ \overline{3}p$	$^5P^o$	379976	60	$2p^3\ \overline{3}s$	$^3D^o$	584855
25	$2s\ 2p^2\ \overline{3}p$	$^3D^o$	392038	61	$2p^3\ \overline{3}s$	$^3S^o$	589631
26	$2s\ 2p^2\ \overline{3}p$	$^5S^o$	395094	62	$2p^3\ \overline{3}p$	^3P	600736
27	$2s\ 2p^2\ \overline{3}p$	$^3P^o$	400796	63	$2s\ 2p^2\ \overline{3}d$	^5F	600824
28	$2s\ 2p^2\ \overline{3}s$	^3P	418063	64	$2p^3\ \overline{3}s$	$^1D^o$	602294
29	$2s\ 2p^2\ \overline{3}p$	$^3F^o$	437947	65	$2p^3\ \overline{3}p$	^1D	606079
30	$2s\ 2p^2\ \overline{3}p$	$^1D^o$	439915	66	$2p^3\ \overline{3}p$	^3S	606299
31	$2s\ 2p^2\ \overline{3}s$	^3D	442045	67	$2p^3\ \overline{3}p$	^3D	607292
32	$2s\ 2p^2\ \overline{3}p$	$^1F^o$	443431	68	$2s\ 2p^2\ \overline{3}d$	^5D	610073
33	$2s\ 2p^2\ \overline{3}p$	$^3D^o$	447068	69	$2p^3\ \overline{3}p$	^1P	612417
34	$2s\ 2p^2\ \overline{3}p$	$^1P^o$	449383	70	$2s^2\ 2p\ \overline{3}d$	$^1P^o$	617417
35	$2s\ 2p^2\ \overline{3}p$	$^3P^o$	456397	71	$2p^3\ \overline{3}p$	^3P	618955
36	$2s\ 2p^2\ \overline{3}s$	^1D	468076	72	$2s^2\ 2p\ \overline{3}d$	$^1F^o$	620437

thresholds for convergence of resonance series. In some cases this required re-ordering the target states.

Collision strengths were calculated for electron energies up to 1.28 Rydberg relative to the $2s^2\ 2p^2\ ^3P_0$ ground level, hence 0.89 Rydberg relative to the highest state of interest, $2s^2\ 2p^2\ ^1S_0$. This energy corresponds to $\approx 7kT$ when the electron temperature $T = 20000$ K, the approximate upper limit for temperatures in photoionized nebulae. Over this energy range, collision strengths were calculated at 20000 equally spaced energies, except between the $2s^2\ 2p^2\ ^3P_1$ and $^3P_2$ levels where calculations were performed on a mesh 100 times finer. Calculations were also made with and without Gailitis averaging of the collision strengths in the region beneath each threshold where the effective quantum number $\nu > 10$.

We calculate the thermodynamically-averaged collision strengths for electron excitation, Υ, from a lower state i to an upper state j from

$$\Upsilon_{i \to j}(\epsilon_i, T_f) = \frac{\sqrt{\pi}}{2} e^{\left(\frac{\Delta E_{ij}}{kT_f}\right)} \int_0^\infty \Omega_{ij}(\epsilon_i) \left(\frac{kT_f}{\epsilon_i}\right)^{1/2} f(\epsilon_i, T_f)\, d\epsilon_j \tag{1}$$

where T_f is the effective temperature, k is the Boltzmann constant, ϵ_i and ϵ_j are the free electron energy relative to the states i and j respectively, $\Delta E_{ij}\ (= \epsilon_i - \epsilon_j)$ is the energy difference between the two states, Ω_{ij} is the collision strength of the transition between the i and j states, and $f(\epsilon_i, T_f)$ is the energy- and temperature-dependent electron distribution. In what follows we will only consider Maxwell-Boltzmann distributions of electron energy, given by

$$f_{MB}(\epsilon, T) = \frac{2}{(kT)^{3/2}} \sqrt{\frac{\epsilon}{\pi}} e^{-\frac{\epsilon}{kT}}, \tag{2}$$

although, as discussed above, other distributions such as the κ distribution have been proposed and discussed (Vasyliunas 1968; Nicholls *et al* 2012; Storey & Sochi 2013).
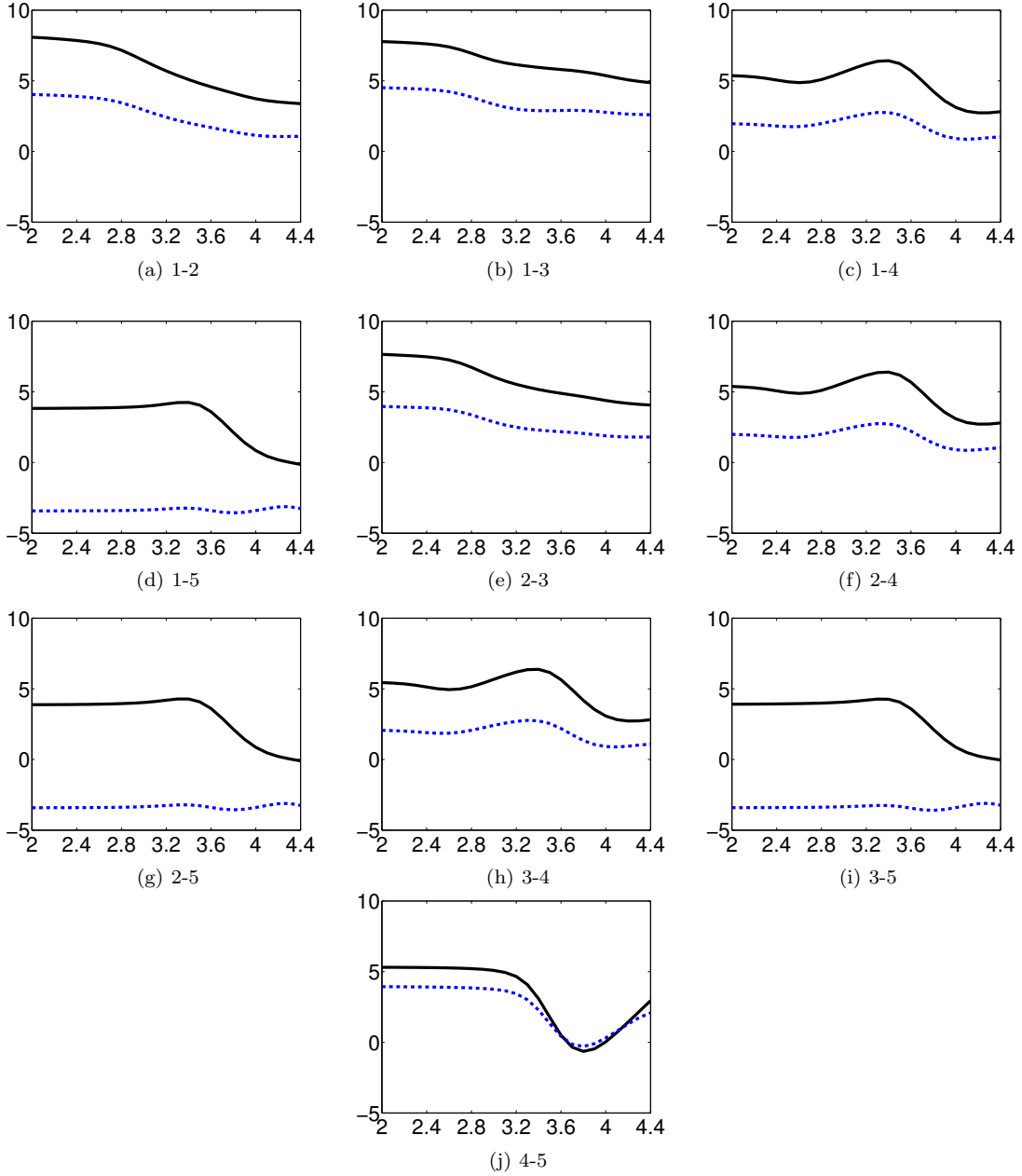
Figure 2. Thermally averaged collision strengths from the 10-term target (solid black line) and 20-term target (dotted blue line), shown as the percentage difference from the 72-term target, plotted against $\log T$ [K]. The labels of the sub-figures refer to the level indices in Table 4.

3 RESULTS AND DISCUSSION

3.1 Results

A sample of our 10-, 20- and 72-term BP collision strengths is shown in Figure 1. The agreement between the three calculations is excellent, with the most obvious difference being that some resonances move to lower energies as the target size is increased, as might be expected. Figure 2 shows the results for the thermally averaged collision strength, Υ, as a function of temperature for the 10- and 20-term calculations relative to the 72-term calculation as a percentage difference. The differences are less than 9% at any temperature for the 10-term calculation and less than 5% for the 20-term case.

The energy region between the $2s^2\ 2p^2\ {}^3P_1$ and ${}^3P_2$ states contains a Rydberg series of resonances converging on the ${}^3P_2$ level with an effective quantum number at the ${}^3P_1$ threshold of 47.7. The energy difference between the ${}^3P_1$ and ${}^3P_2$ levels of 193 cm^{-1} corresponds to a temperature of 278 K, so this energy region is significant for computing Υ at temperatures down to 100 K. We calculate the collision strengths with an energy interval of 6.4×10^{-7} Rydberg in this interval and compare with the result of using Gailitis averaging in this region. The difference is less than 1% at any temperature and we conclude that Gailitis averaging is adequate to obtain accurate values of Υ down to 100 K.

The results of the ICFT calculations showed unexpect-

Table 4. The 18 lowest energy levels of the $n = 2$ complex of O^{2+} and their experimental (E_{ex}) and theoretical (E_{th1} and E_{th2}) energies in wavenumbers (cm^{-1}). Four non-physical states of the configuration $2\mathrm{s}^2\, 2\mathrm{p}\, \overline{3}\mathrm{s}$ are omitted from the list which is indexed in experimental energy order. The experimental energies are obtained from the NIST database while the theoretical energies were obtained from Autostructure with the configuration basis listed in Table 1. The energies E_{th1} were obtained with only spin-orbit terms in the target Hamiltonian while E_{th2} also include two-body fine-structure interactions within the $n = 2$ complex.

Index	Level	E_{ex}	E_{th1}	E_{th2}
1	$2\mathrm{s}^2\, 2\mathrm{p}^2\ ^3\mathrm{P}_0$	0.00	0	0
2	$2\mathrm{s}^2\, 2\mathrm{p}^2\ ^3\mathrm{P}_1$	113.18	115	113
3	$2\mathrm{s}^2\, 2\mathrm{p}^2\ ^3\mathrm{P}_2$	306.17	339	308
4	$2\mathrm{s}^2\, 2\mathrm{p}^2\ ^1\mathrm{D}_2$	20273.27	21489	21471
5	$2\mathrm{s}^2\, 2\mathrm{p}^2\ ^1\mathrm{S}_0$	43185.74	45900	45882
6	$2\mathrm{s}\, 2\mathrm{p}^3\ ^5\mathrm{S}^o_2$	60324.79	59600	59582
7	$2\mathrm{s}\, 2\mathrm{p}^3\ ^3\mathrm{D}^o_3$	120058.2	121800	121775
8	$2\mathrm{s}\, 2\mathrm{p}^3\ ^3\mathrm{D}^o_2$	120053.4	121804	121799
9	$2\mathrm{s}\, 2\mathrm{p}^3\ ^3\mathrm{D}^o_1$	120025.2	121812	121805
10	$2\mathrm{s}\, 2\mathrm{p}^3\ ^3\mathrm{P}^o_2$	142393.5	145316	145307
11	$2\mathrm{s}\, 2\mathrm{p}^3\ ^3\mathrm{P}^o_1$	142381.8	145321	145307
12	$2\mathrm{s}\, 2\mathrm{p}^3\ ^3\mathrm{P}^o_0$	142381.0	145331	145319
13	$2\mathrm{s}\, 2\mathrm{p}^3\ ^1\mathrm{D}^o_2$	187054.0	191025	191006
14	$2\mathrm{s}\, 2\mathrm{p}^3\ ^3\mathrm{S}^o_1$	197087.7	200423	200405
15	$2\mathrm{s}\, 2\mathrm{p}^3\ ^1\mathrm{P}^o_1$	210461.8	215609	215591
⋮	⋮	⋮	⋮	⋮
20	$2\mathrm{p}^4\ ^3\mathrm{P}_2$	283759.7	288653	288629
21	$2\mathrm{p}^4\ ^3\mathrm{P}_1$	283977.4	288863	288854
22	$2\mathrm{p}^4\ ^3\mathrm{P}_0$	284071.9	288965	288951

edly large differences from the BP results in some energy domains. This is illustrated in Figure 3 where we compare the thermally averaged collision strengths for the 72-term ICFT calculations with the 72-term BP results for the $^3\mathrm{P}_1$ − $^3\mathrm{P}_2$ transition. Due to the difference in scaling with effective charge (z_{eff}) of term energy separations ($\propto z_{\mathrm{eff}}$) and resonance energies ($\propto z_{\mathrm{eff}}^2$), resonance effective quantum numbers can become small for lowly ionized systems. Such deeply-closed channels can be problematic for the multichannel quantum defect theory (MQDT) used by the ICFT method due to computational finite numerical precision of highly divergent wavefunctions. Gorczyca & Badnell (2000) found that classically forbidden channels (e.g. $n < l$) could be handled expediently by simply omitting them from the MQDT representation. For low-energy scattering in O^{2+} we encountered a similar problem in a new guise for $n \lesssim 2$. The closed-channel partition of the MQDT representation should give no contribution since all bound orbitals (spectroscopic and pseudo) are projected out of the continuum basis. All such closed channel contributions (e.g. correlation resonances) arise instead in the open-open part of the scattering matrix. For $l > 1$ the original Gorczyca & Badnell (2000) expediency already omits such closed channels ($n < l$). For $l = 0, 1$ we found it necessary to explicitly omit such closed channels from the closed partition as well. We show the effect of this modification as the dashed blue line in Figure 3. The agreement with the full Breit-Pauli calculation is now excellent.

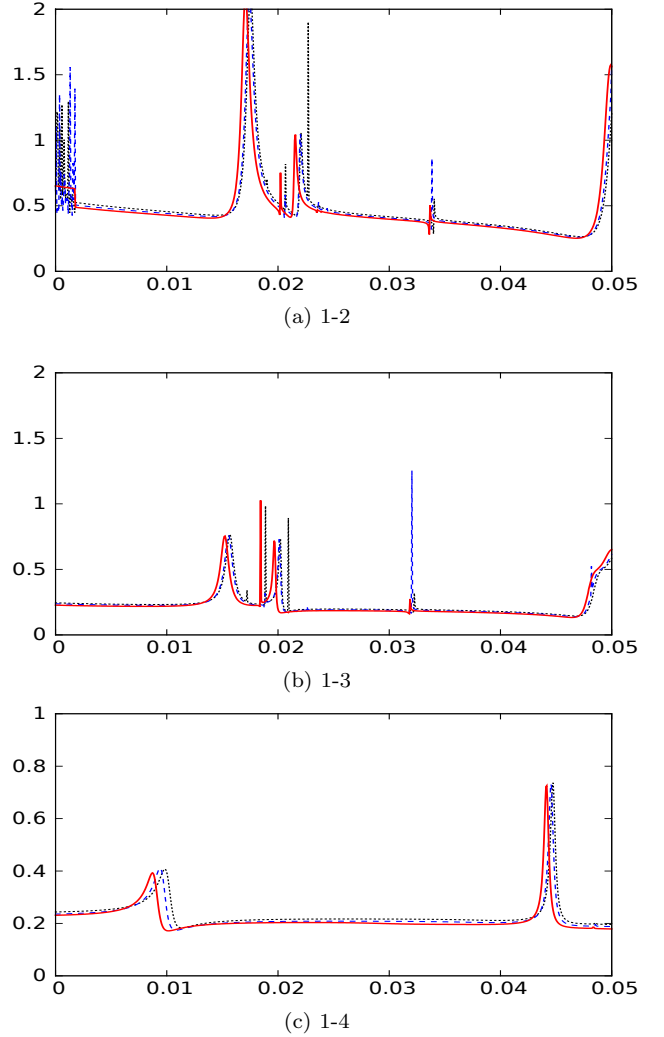Considering the convergence as the number of target

Figure 1. Collision strength (vertical axis) versus final electron energy in Rydberg (horizontal axis) for Breit-Pauli calculations of the 1-2, 1-3 and 1-4 transitions with 10-term (dotted black line), 20-term (dashed blue line), and 72-term (solid red line). Refer to Table 4 for level indexing.

states is increased and the good agreement between the ICFT and Breit-Pauli results, we adopt the results of the 72-term Breit-Pauli calculation as our final results and, based on the convergence behavior and the effect of Gailitis averaging, estimate an uncertainty of no more than 5% in the final thermally averaged collision strengths. In Table 5 we tabulate thermally averaged collision strengths Υ, for the 72-term target in the temperature range $\log_{10} T = 2.0(0.1)4.4$.

3.2 Comparison to Previous Work

We compare our effective collision strength results with those from previous calculations of similar quality, that is those which used close-coupling techniques and computed collision strengths at sufficient energies to delineate resonances.

In Table 6 we compare our final 72-term results with the LS results of Lennon & Burke (1994). That calculation was based on the 12-state target including $n = 3$ correlation orbitals described by Burke, Lennon & Seaton (1989). They

Table 5. Thermally averaged collision strengths from the 72-term Breit-Pauli calculation as a function of temperature. See Table 4 for the transition indices.

log T [K]	1-2	1-3	1-4	1-5	2-3	2-4	2-5	3-4	3-5	4-5
2.0	0.635	0.226	0.232	0.030	1.112	0.697	0.090	1.170	0.151	0.383
2.1	0.626	0.226	0.232	0.030	1.110	0.698	0.090	1.172	0.151	0.383
2.2	0.615	0.225	0.233	0.030	1.107	0.700	0.090	1.174	0.151	0.383
2.3	0.602	0.225	0.233	0.030	1.104	0.702	0.090	1.178	0.151	0.383
2.4	0.587	0.224	0.234	0.030	1.100	0.706	0.090	1.184	0.151	0.384
2.5	0.572	0.224	0.236	0.030	1.095	0.710	0.090	1.191	0.151	0.384
2.6	0.557	0.224	0.238	0.030	1.092	0.715	0.090	1.199	0.151	0.385
2.7	0.543	0.225	0.239	0.030	1.093	0.719	0.090	1.206	0.151	0.386
2.8	0.532	0.226	0.239	0.030	1.098	0.720	0.090	1.208	0.150	0.387
2.9	0.524	0.229	0.239	0.030	1.109	0.718	0.089	1.205	0.150	0.388
3.0	0.520	0.231	0.237	0.030	1.122	0.713	0.089	1.197	0.150	0.390
3.1	0.517	0.233	0.234	0.030	1.134	0.705	0.089	1.184	0.149	0.392
3.2	0.515	0.235	0.231	0.029	1.143	0.696	0.088	1.168	0.148	0.397
3.3	0.514	0.236	0.228	0.029	1.150	0.686	0.088	1.152	0.148	0.405
3.4	0.513	0.237	0.225	0.029	1.156	0.677	0.087	1.137	0.147	0.420
3.5	0.514	0.238	0.223	0.029	1.163	0.672	0.087	1.129	0.146	0.445
3.6	0.516	0.240	0.223	0.029	1.174	0.673	0.088	1.131	0.147	0.480
3.7	0.520	0.242	0.227	0.030	1.187	0.682	0.089	1.148	0.150	0.521
3.8	0.526	0.246	0.232	0.030	1.206	0.700	0.091	1.177	0.154	0.562
3.9	0.534	0.251	0.240	0.031	1.228	0.724	0.095	1.217	0.159	0.596
4.0	0.542	0.257	0.249	0.033	1.253	0.751	0.098	1.262	0.166	0.617
4.1	0.550	0.263	0.258	0.034	1.277	0.778	0.102	1.307	0.172	0.627
4.2	0.555	0.270	0.267	0.035	1.299	0.803	0.106	1.348	0.178	0.625
4.3	0.559	0.277	0.274	0.036	1.319	0.825	0.109	1.385	0.184	0.616
4.4	0.561	0.283	0.280	0.037	1.338	0.842	0.112	1.414	0.188	0.602
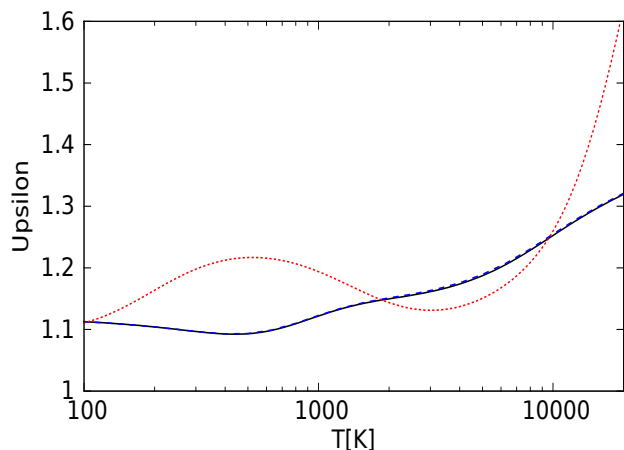
Figure 3. Effective collision strength (Upsilon) versus temperature from the 72-term target: Breit-Pauli (solid black line), ICFT before modification (dotted red line) and ICFT after modification (dashed blue line), for the transition between levels 2 and 3 of Table 4. On this scale the solid and dashed lines are almost indistinguishable.

agree within 10% for all transitions and all temperatures. The effective collision strengths, $\Upsilon(^3P - {}^1D)$ and $\Upsilon(^3P - {}^1S)$, for excitation of the optical forbidden lines do not differ by more than 6% at any temperature. The agreement is generally even better with our 20-term calculation which might be expected since that calculation includes the 12 terms of the $n = 2$ complex which is the target of Lennon & Burke (1994). However, their target does not include the states constructed from correlation orbitals that make a large con-

tribution to the polarizability of the important states, as discussed in section 2.1.

The most recent R-matrix calculations where fine-structure collision strengths are presented are those of Aggarwal & Keenan (1999) and Palay *et al* (2012). The former calculation is based on an elaborate 26-term target described by Aggarwal & Hibbert (1991) constructed from 1s, 2s and 2p spectroscopic and 3s, 3p, 3d, 4s, 4p and 4d correlation orbitals. The resulting LS-coupled reactance matrices were recoupled algebraically using the JAJOM (Saraph 1978) program where necessary. This approach neglects the fine-structure interactions between target states and in this approximation some fine-structure collision strengths can be derived directly from LS-coupled collision strengths using only statistical weight factors as described by both Aggarwal & Keenan (1999) and Lennon & Burke (1994). Palay *et al* (2012) have made a 19-level Breit-Pauli R-matrix calculation where the target is expanded over a configuration set involving 1s, 2s, 2p and 3s spectroscopic orbitals and 3p, 3d, 4s and 4p correlation orbitals. Palay *et al* (2012) use an extended version of the Breit-Pauli R-matrix code which they attribute to Eissner & Chen (in preparation) that includes two-body fine-structure interactions which enables Palay *et al* (2012) to calculate the fine structure splitting of the ground ^3P_J levels with an error of order 3%. Palay *et al* (2012) were also the first to extend the tabulation of thermally averaged collision strengths down to very low electron temperatures (100 K).

In Figure 4 we compare graphically our fine-structure results with those of Lennon & Burke (1994), Aggarwal & Keenan (1999) and Palay *et al* (2012). In Table 7 we compare the same results numerically and also include the results of

the earlier R-matrix calculation by Aggarwal (1983). Figure 4 shows the percentage difference in the thermally averaged collision strengths from these three calculations relative to our results, for all ten transitions among the energetically lowest five levels. Where necessary, we derived fine-structure collision strengths from the results of Lennon & Burke (1994) and Aggarwal & Keenan (1999) using statistical weight factors as outlined above. With the exception of the $^1D_2 - {}^1S_0$ transition, our results agree with those of Lennon & Burke (1994) and Aggarwal & Keenan (1999) to within 10% for all temperatures between 1000 K and 25000 K where comparison can be made and to within 5% for the majority of temperatures. For these two calculations the differences are relatively insensitive to temperature, indicating that their collision strengths have a similar energy dependence to ours. We find generally larger disagreements with the results of Palay *et al* (2012), reaching 10–15% at the extremes of tabulated temperature for many transitions and being even larger for the transitions from the ground ^3P_J levels to the $^1S_0$ state (transitions 1-5, 2-5 and 3-5). Here the differences reach 100% at 100 K and are over 20% at 10000 K. The differences also show a distinctive temperature dependence. With the exception of the $^3P_J - {}^1S_0$ transitions the Palay *et al* (2012) results are generally smaller than ours at the lowest temperatures and larger at the highest temperatures.

In Figure 6 we compare collision strengths from Palay *et al* (2012) with our 72-term target for the transitions, $^3P_2 - {}^1S_0$ and $^3P_2 - {}^1D_2$, over an energy range that includes the $^1S_0$ threshold. For the $^3P_2 - {}^1S_0$ transition the results of Palay *et al* (2012) are generally larger near the threshold and rise sharply as the threshold is approached, being approximately a factor of two larger than our results at the threshold. This behavior, which is replicated for the $^3P_0 - {}^1S_0$ and $^3P_1 - {}^1S_0$ transitions, explains the large differences seen in Figure 4 and Figure 8 for the thermally averaged collision strengths at the lowest temperatures. The plot of the $^3P_2 - {}^1D_2$ collision strength shows that there is a resonance feature just below the $^1S_0$ threshold in the results of Palay *et al* (2012) that is not present in our 72-term results which might be the cause of the sharp rise seen at threshold in their $^3P_2 - {}^1S_0$ collision strength. We note that Palay *et al* (2012) omitted the three $2p^4$ terms from their scattering target, although it was included in their configuration expansion. This raises the possibility that the $O^+ 2p^5$ state, which is presumably represented by an (N+1)-electron state composed only of target orbitals in their calculation, is not accurately described and is the cause of the feature seen just below the $^1S_0$ threshold and hence of the large difference compared to our, and other calculations.

We attempted to confirm this possibility by making two simple test calculations, one with all 12 terms of the $n = 2$ complex in the target and one with the three terms of the $2p^4$ configuration omitted as in the Palay *et al* (2012) calculation. This latter 9-term target does not show the resonance feature seen in their results just below the $^1S_0$ threshold nor the sharp rise in the $^3P_J - {}^1S_0$ collision strengths at threshold. To clarify the position of the $2p^5$ $^2P^o$ state in these calculations we also calculated photoionization cross-sections from $O^+ 2s\, 2p^4\, {}^2D_{3/2}$ which is expected to show prominent resonances corresponding to the $2s\, 2p^4\, {}^2D_{3/2} - 2p^5\, {}^2P^o_{1/2,3/2}$ transitions. In the 12-term calculation the $2p^5\, {}^2P^o_{1/2,3/2}$ states are found at 0.3166 and 0.3145 Rydberg, well below the $^1S_0$ threshold, while in the 9-term calculation they lie at 0.4371 and 0.4379 Rydberg, well above it. Given that the Palay *et al* (2012) calculation omits the $2p^4$ target terms but includes other correlation in the configuration expansion it is at least plausible that the resonance feature just below the $^1S_0$ threshold is indeed due to the misplaced $2p^5$ levels. Incidentally, the $^3P_2 - {}^1D_2$ collision strengths from our 72-term calculation in Figure 6 shows a minor series perturbation near 0.315 Rydberg that probably corresponds to $2p^5\, {}^2P^o$.

3.3 Discussion

In photoionized plasmas the O III forbidden lines are commonly used to determine the electron temperature of the emitting material, and hence to determine the number of O^{2+} emitters relative to H by comparison with a strong H recombination line. The temperature determination rests on the ratio of the intensity of the $\lambda 4363$ line to either or both of the $\lambda 4959$ and $\lambda 5007$ lines. The $\lambda 4363$ line is relatively weak and cannot be seen if the temperature is much below 5000 K. Once the temperature is known, the much stronger $\lambda\lambda 4959, 5007$ lines can be used to deduce the O^{2+} number density. In nebular plasmas all these lines are excited collisionally from the ^3P_J ground levels. The excitation mechanism for $\lambda 4363$ is therefore central to determining the electron temperature and abundances. In Figure 5 we show how the derived electron temperature from our work differs from that obtained from Lennon & Burke (1994) and from the data of Aggarwal & Keenan (1999) and Palay *et al* (2012). In all the temperature determinations the radiative transition probabilities were taken from Nussbaumer & Storey (1981) and Storey & Zeippen (2000). Very similar temperatures are obtained with the collision strength data of Lennon & Burke (1994) and Aggarwal & Keenan (1999). Palay *et al* (2012) state that there are no significant differences in line ratios arising from their calculation when comparing to Aggarwal & Keenan (1999) but Figure 5 shows that this is not the case. The difference in derived temperature is 213 K at 5000 K, 421 K at 10000 K and 504 K at 15000 K.

In summary, our new Breit-Pauli R-matrix calculation generally shows much better agreement for thermally averaged collision strength with the earlier non-Breit-Pauli R-matrix calculations of Lennon & Burke (1994) and Aggarwal & Keenan (1999) than the more recent Breit-Pauli work of Palay *et al* (2012). The results of the important forbidden line diagnostic line ratios show the same pattern. One question that arises is whether the two-body fine-structure terms that are included in the Breit-Pauli R-matrix formulation of Palay *et al* (2012) and not in our calculation might be part of the cause. We do not believe that this is the case for the following reason. In Figure 7 we show two sets of results for the thermally averaged collision strength for the $^3P_1 - {}^3P_2$ transition from 72-term ICFT calculations. The solid line includes the effects of the spin-orbit interaction in the target, introduced *via* the so-called Term-Coupling Coefficients (TCCs), while the dashed line shows the results obtained in pair-coupling, i.e. without TCCs. Except at the lowest temperatures ($T < 300$ K) they differ by no more than 1%. The larger difference at the lowest temperatures simply reflects
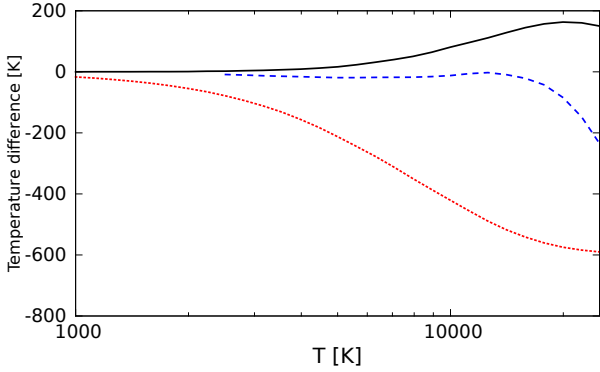
Figure 5. The difference in derived electron temperature from the $\lambda4363/(\lambda4959+\lambda5007)$ line intensity ratio using the data of Lennon & Burke (1994) (solid black line), Aggarwal & Keenan (1999) (dashed blue line) and Palay *et al* (2012) (dotted red line) against the temperature derived from the present results.
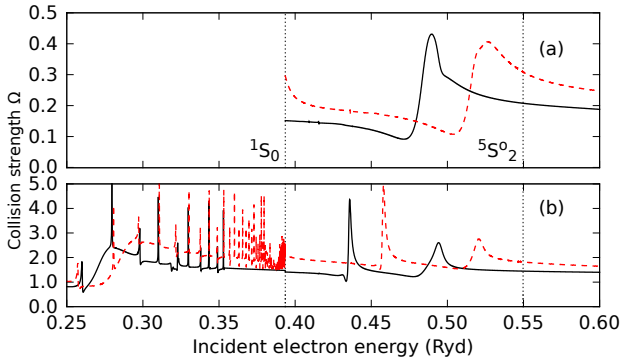

Figure 7. Effective collision strength (Upsilon) versus temperature from 72-term target for the $^3P_1 - {}^3P_2$ transition: ICFT with spin-orbit interactions in the target (solid black line) and ICFT in pair coupling (dashed blue line).

Figure 6. Collision strengths as a function of incident electron energy for (a) the $^3P_2-{}^1S_0$ and (b) the $^3P_2-{}^1D_2$ transitions near the $^1S_0$ threshold from the present 72-term target (solid black line) and from Palay *et al* (2012) (red dashed line). The vertical dotted lines indicate the positions of the $^1S_0$ and $^5S^o_2$ thresholds.

Figure 8. Percentage difference in Υ versus logarithm of temperature between the results of Palay *et al* (2012) and our 72-term Breit-Pauli calculation for the transitions $^3P_0-{}^1S_0$ (black triangle), $^3P_1-{}^1S_0$ (blue circle) and $^3P_2-{}^1S_0$ (red square).

4 CONCLUSIONS

In the present paper, the collision strengths for the transitions between the lowest five levels of the astronomically-important $O^{2+} + e^-$ atomic system up to about 1.3 Rydberg of electron excitation energy are computed in the close coupling approximation using the UCL-Belfast-Strathclyde R-matrix atomic code. Different coupling schemes with different atomic definitions and parameters are used to describe the scattering target and scattering process.

Our results were extensively compared to previous work. We found a good agreement in most cases which increases our confidence in our results. However, we found significant differences with Palay *et al* (2012) who also used a Breit-Pauli coupling scheme and hence a better agreement was expected. The good agreement between our R-matrix Breit-Pauli calculation and earlier R-matrix work in which the fine-structure was treated more approximately strongly supports our results. We showed that the relatively large differences found for the excitation of the $\lambda4363$ line between the work of Palay *et al* (2012) on the one hand, and all previ-

the fact that the pair-coupling calculation does not separate the ^3P_J levels in energy and therefore the threshold energies of these levels are not correct. The results for the other transitions show similar behavior. We emphasize, however, that the ICFT calculation which does incorporate target spin-orbit effects agrees with the full Breit-Pauli calculation to within 1% at all temperatures. The good agreement that we find shows that the spin-orbit interaction has a very small effect on the results. In O^{2+} two-body fine-structure interactions are substantially smaller than the spin-orbit interaction and should therefore have a negligible effect on the results. This point is emphasized in Figure 8 where we show the percentage difference between the results of Palay *et al* (2012) and ours for the three $^3P_J - {}^1S_0$ transitions. Except at very low temperatures, they do not show any significant dependence on J which might be expected if fine-structure effects were important and indicate rather that the term-term $^3P - {}^1S$ collision strengths differ significantly between the two calculations.
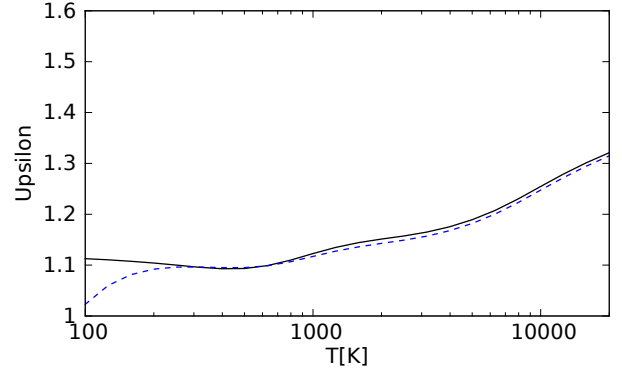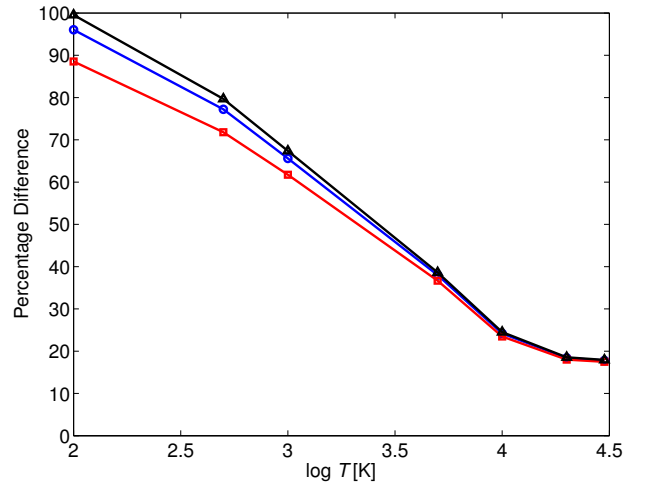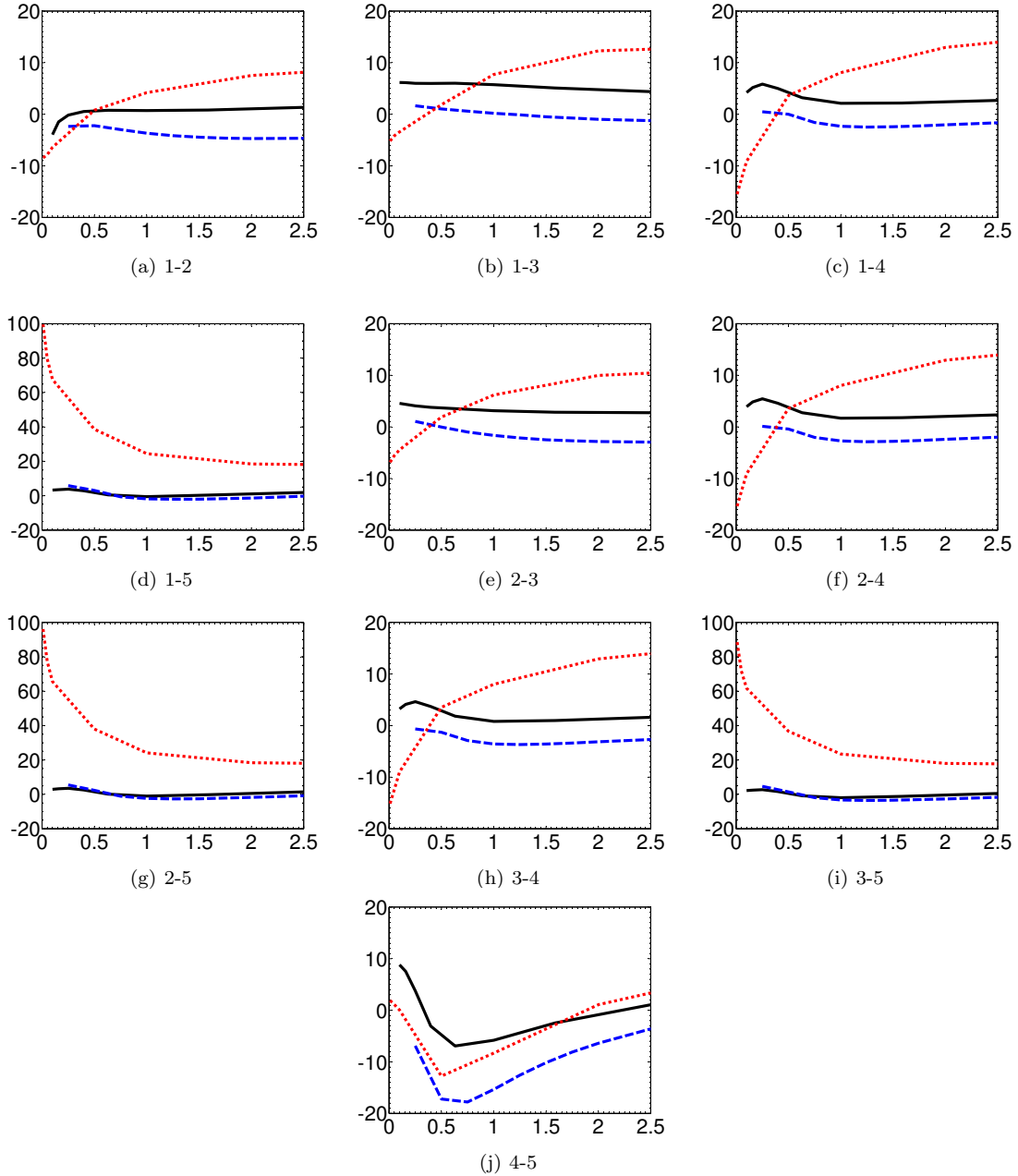
Figure 4. Percentage differences of thermally averaged collision strengths from our 72-term Breit-Pauli calculation (vertical axis) versus temperature in 10000 K (horizontal axis). Results are from Lennon & Burke (1994) (solid black line), Aggarwal & Keenan (1999) (dashed blue line) and Palay *et al* (2012) (dotted red line). The labels of the sub-figures refer to the level indices in Table 4.

ous calculations, on the other, leads to significant differences in derived temperatures from the main [O III] line ratios.

With regard to the use of the ICFT method, for lowly ionized systems some resonances can have very low principal quantum number, and channels are deeply closed, which can cause problems for multichannel quantum defect theory. This difficulty can be overcome by explicitly omitting channels with very low effective quantum number and in any case evaporates as the effective charge number increases.

5 ACKNOWLEDGMENTS AND STATEMENT

REFERENCES

Aggarwal K.M., 1983, ApJS, 52, 387

Aggarwal K.M., 1985, A&A, 146, 149

Aggarwal K.M., Hibbert A., 1991, J. Phys. B, 24, 3445

Aggarwal K.M., 1993, ApJS, 85, 197

Aggarwal K.M., Keenan F.P., 1999, ApJS, 123, 311

Badnell N.R., 2011, Comput. Phys. Commun., 182, 1528

Baluja K.L., Burke P.G., Kingston A.E., 1980, J. Phys. B, 13, 829

Berrington K.A., Burke P.G., Chang J.J., Chivers A.T., Robb W.D., Taylor K.T., 1974, Comp. Phys. Comm., 8, 149

Berrington K.A., Burke P.G., Butler K., Seaton M.J., Storey P.J., Taylor K.T., Yu Yan., 1987, J. Phys. B, 20, 6379

Berrington K.A., Eissner W.B., Norrington P.H., 1995, Comp. Phys. Comm., 92, 290

Bhatia A.K., Doschek G.A., Feldman U., 1979, A&A, 76, 359

Bohm D., Aller L.H., 1947, ApJ, 105, 131

Burke V.M., Lennon, D.J., Seaton, M.J., 1989, MNRAS, 236, 353

Czyzak S.J., Krueger T.K., de Martins P.A.P., Saraph H.E., Seaton M.J., Shemming J., 1968, In Planetary Nebulae by Osterbrock D.E. and O'Dell C.R. (Editors), 34, 138

Eissner W., Jones M., Nussbaumer H., 1974, Comp. Phys. Comm., 8, 270

Gorczyca T.W., Badnell N.R. 2000, J. Phys. B, 33, 2955

Griffin D.C., Badnell N.R., Pindzola M.S., 1998, J. Phys. B, 31, 3713

Hagihara Y., 1944, Proceedings of the Japan Academy, 20, 493

Hibbert A., 1975, Comp. Phys. Comm., 9, 141

Ho Y.K., Henry R.J.W., 1983, ApJ, 264, 733

Hummer D.G., Berrington K.A., Eissner W., Pradhan A.K., Saraph H.E., Tully J.A., 1993, A&A, 279, 298

Lennon D.J., Burke V.M., 1994, A&AS, 103, 273

Liu X.-W., Storey P.J., Barlow M.J., Danziger I.J., Cohen M., Bryce M., 2000, MNRAS, 312, 585

Liu X.-W., Barlow M.J., Zhang Y., Bastin R.J., Storey P.J., 2006, MNRAS, 368, 1959

Maiolino R., Nagao T., Grazian A., *et al*, 2008, A&A, 488, 463

Nicholls D.C., Dopita M.A., Sutherland R.S., 2012, ApJ, 752, 148

Nussbaumer H., Storey P.J., 1978, A&A, 64, 139

Nussbaumer H., Storey P.J., 1981, A&A, 99, 177

Palay E., Nahar S.N., Pradhan A.K., Eissner W., 2012, MNRAS Let., 423, L35

Saraph, H.E., 1978, Comp. Phys. Comm., 15, 247

Seaton M.J., 1975, MNRAS, 170, 475

Sochi T., 2012, PhD thesis, University College London

Sochi T., Storey P.J., 2013, Atomic Data and Nuclear Data Tables, 99, 633

Storey P.J., Zeippen C.J., 2000, MNRAS 312, 813

Storey P.J., Sochi T., 2013, MNRAS, 430, 599

Storey P.J., Sochi T., 2014, MNRAS, 440, 2581

Vasyliunas V.M., 1968, Journal of Geophysical Research, 73, 2839

Zhang Y., Liu X.-W., Wesson R., Storey P.J., Liu Y.,

Danziger I.J., 2004, MNRAS, 351, 935

Table 6. Comparison of thermally averaged collision strengths, Υ, from Lennon & Burke (1994) (LB) and the current work within the lowest five levels of O^{2+} as a function of temperature. The first row of each temperature is from Table 3 of LB and the second row is from the current work using the Breit-Pauli 72-term target. The values given for ^3P-$^1D_2$ and ^3P-$^1S_0$ are summed over the ^3P_J levels.

$\log T$ [K]	$^3P_0$-$^3P_1$	$^3P_0$-$^3P_2$	$^3P_1$-$^3P_2$	^3P-$^1D_2$	^3P-$^1S_0$	$^1D_2$-$^1S_0$
3.0	0.4975	0.2455	1.1730	2.2233	0.2754	0.4241
	0.5199	0.2313	1.1218	2.1331	0.2667	0.3897
3.2	0.5066	0.2493	1.1930	2.1888	0.2738	0.4268
	0.5154	0.2349	1.1430	2.0811	0.2643	0.3968
3.4	0.5115	0.2509	1.2030	2.1416	0.2713	0.4357
	0.5132	0.2367	1.1558	2.0237	0.2610	0.4200
3.6	0.5180	0.2541	1.2180	2.1117	0.2693	0.4652
	0.5158	0.2398	1.1736	2.0107	0.2616	0.4799
3.8	0.5296	0.2609	1.2480	2.1578	0.2747	0.5232
	0.5260	0.2462	1.2057	2.0913	0.2732	0.5621
4.0	0.5454	0.2713	1.2910	2.2892	0.2925	0.5815
	0.5421	0.2568	1.2526	2.2425	0.2941	0.6174
4.2	0.5590	0.2832	1.3350	2.4497	0.3174	0.6100
	0.5551	0.2698	1.2994	2.3987	0.3165	0.6254
4.4	0.5678	0.2955	1.3730	2.5851	0.3405	0.6090
	0.5609	0.2835	1.3378	2.5184	0.3339	0.6022

Table 7. Comparison of thermally averaged collision strengths, Υ, between Aggarwal (1983) (A), Lennon & Burke (1994) (LB), Aggarwal & Keenan (1999) (AK), Palay *et al* (2012) (P), and the current work (SSB) using the 72-term target as a function of temperature [K]. See Table 4 for the transition indices. Note that the values attributed to Lennon & Burke (1994) for $T = 2500$ K and 25000 K are those tabulated for $\log T = 3.4$ and 4.4 in that work respectively.

Index		100	500	1000	2500	5000	7500	10000	12500	15000	17500	20000	25000	30000
								Temperature [K]						
1-2	A				0.5041	0.5172	0.5310	0.5417	0.5490	0.5537	0.5567	0.5586	0.5612	0.5633
	LB			0.4975	0.5115			0.5454					0.5678	
	AK			0.5011		0.5084	0.5159	0.5222	0.5266	0.5294	0.5311	0.5324	0.5348	0.5380
	P	0.5814	0.5005	0.4866		0.5240		0.5648				0.6007		0.6116
	SSB	0.6350	0.5430	0.5199	0.5132	0.5199	0.5317	0.5421	0.5494	0.5540	0.5569	0.5587	0.5609	0.5623
1-3	A				0.2499	0.2566	0.2646	0.2717	0.2776	0.2824	0.2865	0.2901	0.2962	0.3013
	LB			0.2455	0.2509			0.2713					0.2955	
	AK			0.2406		0.2449	0.2512	0.2573	0.2626	0.2669	0.2707	0.2739	0.2798	0.2855
	P	0.2142	0.2153	0.2234		0.2469		0.2766				0.3106		0.3264
	SSB	0.2259	0.2247	0.2313	0.2367	0.2424	0.2497	0.2568	0.2629	0.2682	0.2727	0.2766	0.2833	0.2890
1-4	A				0.2283	0.2262	0.2337	0.2426	0.2506	0.2627	0.2627	0.2672	0.2740	0.2790
	LB			0.2470	0.2380			0.2544					0.2872	
	AK			0.2260		0.2265	0.2343	0.2434	0.2515	0.2582	0.2637	0.2683	0.2751	0.2799
	P	0.1959	0.2088	0.2154		0.2347		0.2693				0.3094		0.3256
	SSB	0.2318	0.2389	0.2370	0.2249	0.2265	0.2381	0.2492	0.2579	0.2646	0.2698	0.2739	0.2797	0.2832
1-5	A				0.0278	0.0280	0.0295	0.0310	0.0324	0.0335	0.0344	0.0351	0.0362	0.0368
	LB			0.0306	0.0301			0.0325					0.0378	
	AK			0.0307		0.0304	0.0310	0.0321	0.0332	0.0342	0.0351	0.0358	0.0370	0.0378
	P	0.0597	0.0535	0.0496		0.0409		0.0407				0.0430		0.0442
	SSB	0.0299	0.0298	0.0296	0.0290	0.0295	0.0312	0.0327	0.0339	0.0349	0.0357	0.0363	0.0371	0.0375
2-3	A				1.1925	1.2239	1.2592	1.2884	1.3107	1.3275	1.3404	1.3510	1.3679	1.3821
	LB			1.1730	1.2030			1.2910					1.3730	
	AK			1.1680		1.1870	1.2100	1.2320	1.2490	1.2620	1.2730	1.2820	1.2980	1.3150
	P	1.0360	1.0320	1.0720		1.2100		1.3300				1.4510		1.4990
	SSB	1.1121	1.0928	1.1218	1.1557	1.1873	1.2221	1.2526	1.2763	1.2943	1.3082	1.3194	1.3374	1.3518
2-4	A				0.6848	0.6785	0.7010	0.7279	0.7518	0.7716	0.7879	0.8014	0.8221	0.8368
	LB			0.7411	0.7139			0.7631					0.8617	
	AK			0.6780		0.6795	0.7029	0.7302	0.7545	0.7746	0.7911	0.8049	0.8253	0.8397
	P	0.5903	0.6285	0.6483		0.7067		0.8108				0.9313		0.9802
	SSB	0.6975	0.7187	0.7132	0.6772	0.6823	0.7175	0.7506	0.7768	0.7969	0.8125	0.8247	0.8421	0.8527
2-5	A				0.0833	0.0840	0.0884	0.0931	0.0972	0.1006	0.1033	0.1054	0.1085	0.1105
	LB			0.0918	0.0904			0.0975					0.1135	
	AK			0.0921		0.0911	0.0929	0.0962	0.0995	0.1025	0.1052	0.1074	0.1109	0.1135
	P	0.1765	0.1590	0.1477		0.1228		0.1223				0.1294		0.1332
	SSB	0.0900	0.0897	0.0892	0.0873	0.0890	0.0939	0.0985	0.1022	0.1052	0.1075	0.1093	0.1118	0.1131
3-4	A				1.1413	1.1308	1.1683	1.2131	1.2529	1.2860	1.3132	1.3357	1.3702	1.3947
	LB			1.2352	1.1898			1.2718					1.4362	
	AK			1.1300		1.1325	1.1715	1.2170	1.2575	1.2910	1.3185	1.3415	1.3755	1.3995
	P	0.9934	1.0560	1.0890		1.1880		1.3630				1.5640		1.6450
	SSB	1.1702	1.2057	1.1965	1.1374	1.1474	1.2066	1.2620	1.3055	1.3389	1.3647	1.3850	1.4137	1.4310
3-5	A				0.1388	0.1401	0.1473	0.1552	0.1620	0.1676	0.1721	0.1757	0.1809	0.1842
	LB			0.1530	0.1507			0.1625					0.1892	
	AK			0.1536		0.1518	0.1549	0.1603	0.1659	0.1709	0.1753	0.1790	0.1849	0.1891
	P	0.2850	0.2587	0.2421		0.2045		0.2046				0.2170		0.2235
	SSB	0.1512	0.1506	0.1497	0.1467	0.1496	0.1579	0.1657	0.1720	0.1769	0.1808	0.1839	0.1881	0.1902
4-5	A				0.4708	0.5463	0.6114	0.6468	0.6630	0.6687	0.6692	0.6670	0.6599	0.6524
	LB			0.4241	0.4357			0.5815					0.6090	
	AK			0.3907		0.4312	0.4836	0.5227	0.5478	0.5629	0.5719	0.5769	0.5809	0.5812
	P	0.3900	0.3899	0.3899		0.4544		0.5661				0.6230		0.6219
	SSB	0.3827	0.3856	0.3897	0.4196	0.5208	0.5882	0.6174	0.6266	0.6265	0.6223	0.6163	0.6026	0.5886